Radiation Protection Dosimetry (2004), Vol. 110, Nos 1-4, pp. 789–799
doi:10.1093/rpd/nch171

RECENT ADVANCES OF NANODOSIMETRY

B. Grosswendt
Physikalisch-Technische Bundesanstalt, Department 'Fundamentals of Dosimetry', Bundesallee 100, D-38116 Braunschweig, Germany

The early damage to genes and cells due to ionizing radiation is initiated by the overlay of the track structure of charged particles and of the structure of radiosensitive sub-cellular volumes. As a result of this overlay, a specified number of ionizations (the ionization cluster size) is formed per primary particle. Therefore, one of the aims of nanodosimetry is to determine ionization cluster-size distributions in nanometric volumes of liquid water, as a substitute to sub-cellular structures. After a short description of the main aspects of cluster-size formation by charged particles, an overview of the advanced measuring techniques that use millimetric target volumes filled with a low-pressure gas to simulate nanometric target volumes at unit density is given. Afterwards, physical principles are discussed which are applicable to convert ionization cluster-size distributions measured in gases into those for liquid water. Finally, a tentative possibility is proposed of how to relate parameters derived from cluster-size distributions in liquid water to parameters derived from radiation-induced radiobiological experiments.

INTRODUCTION

The early damage to genes and cells by ionizing radiation starts with the early damage to radiosensitive sub-cellular structures. Here, the so-called clustered damage in segments of the DNA is of particular importance, as pointed out by Goodhead[1]. This clustered damage, which may lead to mutagenic, genotoxic or other potentially lethal lesions such as single-strand or double-strand breaks, can be assumed to be caused by the combination of primary or secondary particle interaction processes in the DNA and successive reactions of damaged sites with reactive species (for instance, OH radicals) produced by ionizing particles within the neighbourhood of DNA. Due to the complexity of radiation-induced damage, our present knowledge on this topic almost exclusively stems from the Monte Carlo simulations based on more or less highly sophisticated models of DNA and on cross section sets for water vapour or liquid water. For an overview of computational modelling of DNA damage, see, for instance, the publications by Nikjoo *et al.*[2] and Friedland *et al.*[3]. The geometrical models of DNA applied in such simulations vary from simple homogeneous linear cylinders to highly sophisticated atomic models which even include higher order structures of DNA such as nucleosomes and chromatin fibre loops. In most of these simulations, radiation-induced damage is calculated by analysing the overlay of particle track structure in liquid water with the geometrical structure of the DNA model. The main result is that radiation damage strongly depends on radiation quality and cannot be described satisfactorily by macroscopic quantities like absorbed dose, which neither take into account the track structure of ionizing particles nor the structure of radiosensitive sub-cellular targets. Therefore, one of the challenges of nanodosimetry is to define a more appropriate physical quantity which is, first, easily measurable and is, second, based on particle interactions in nanometric sites, and thus behaves as a function of radiation quality similar to radiation-induced effects. In the case of success, this physical quantity could be used in the future as the basis for radiation protection dosimetry and also for a more sophisticated radiation treatment, in particular, in the field of heavy ion therapy.

An encouraging starting point to tackle this challenge is, for instance, the finding of Brenner and Ward[4] that the yields of clusters of multiple ionizations produced by ionizing radiation of different quality within sites, 2–3 nm in size, correlate well with yields observed for double-strand breaks. In view of this fact, one of the aims of current nanodosimetry is to develop experimental procedures, which can be applied for measuring the frequency distribution of ionization cluster size (number of ionizations per primary particle) in volumes comparable in size to segments of DNA or chromatin fibre due to the interaction of primary or secondary particles.

The most successful method applied for this purpose is based, at present, on single-particle detection. This method uses highly sophisticated counters filled with gases at low operating pressure to simulate target volumes of mass per area in a size of about 1 μg cm^{-2}, which corresponds to 10 nm at a density of 1.0 g cm^{-3}. The method used in current nanodosimetry is, therefore, the same as that applied in traditional microdosimetry for many years, but is extended to much smaller, simulated target volumes. Here, a great progress has been made since 1995 with respect to the improvement of measuring

Corresponding author: Bernd.Grosswendt@ptb.de

techniques [Pszona *et al.*[5], De Nardo *et al.*[6], Garty *et al.*[7]] and, in particular, also regarding the general understanding of ionization cluster-size formation [De Nardo *et al.*[8]]. At the moment, three different measuring devices are working which use cylindrical target volumes with diameters of mass per area of between ~0.1 and 2.5 μg cm^{-2}, thus covering the sizes of sub-cellular structures such as segments of the DNA or of the chromatin fibre.

The problem of measurements in gaseous systems is that their results cannot be directly applied to biological systems because radiation interaction in gases that are well suited for proportional counter experiments is quite different from that in sub-cellular material. Based on general principles, however, they can be traced back to data for nanometric volumes of liquid water, as a substitute to sub-cellular structures. It is, therefore, the aim of the present paper (i) to summarize the main principles of ionization cluster-size formation in nanometric targets, (ii) to give a short overview on recently used measuring devices, (iii) to apply the general principles of cluster-size formation for developing methods that are applicable to relate the results of gaseous measurements into those for liquid water, and (iv) to propose a tentative procedure on how to apply cluster-size distributions for nanometric targets to radiobiological effects.

GENERAL ASPECTS OF IONIZATION CLUSTER-SIZE FORMATION

Following the concept of De Nardo *et al.*[8] in their analysis of general aspects of the formation of ionization cluster sizes, let $P_\nu(Q;d)$ be the probability that exactly a number ν of ionizations is produced within a specified cylindrical target volume by a single primary particle of radiation quality Q (particle type, energy, ...), passing the volume at a distance d to its main axis (Figure 1). This number of ionizations produced by a primary particle (including its secondary electrons) within the target volume is the so-called cluster size. The latter is the result of a superposition of the ionization component of the particle track structure and of the geometric characteristics of the target volume. The distribution of the probability $P_\nu(Q;d)$ with respect to the formation of cluster size ν, therefore, describes the stochastic nature of the conjunction of track structure and target volume. In consequence, the $P_\nu(Q;d)$-distribution and its moments $M_\xi(Q;d)$ may strongly depend on type and energy of the primary particle, on the

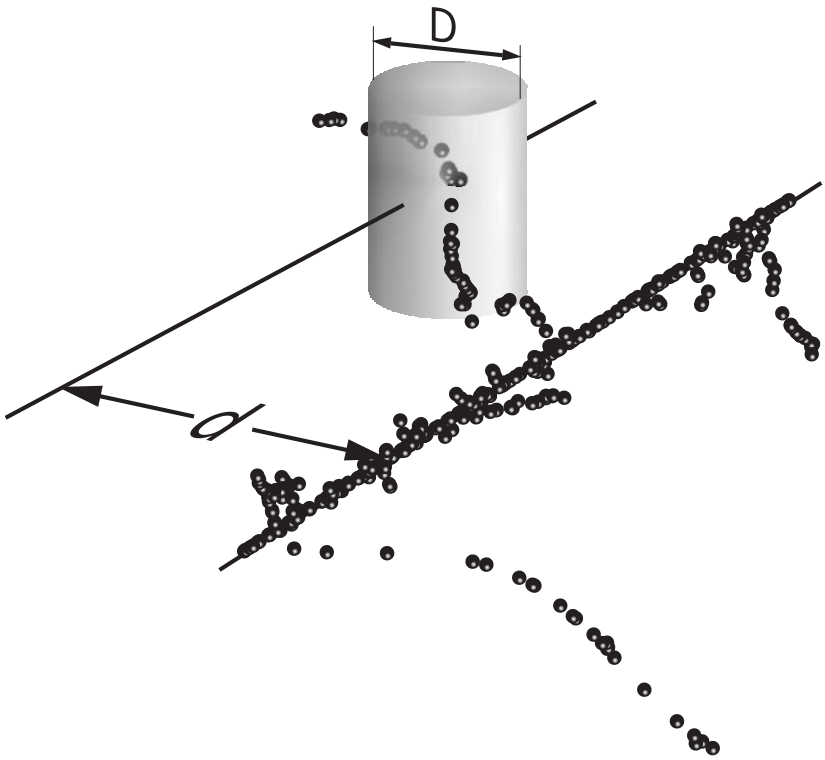

Figure 1. Ionization cluster-size formation by a primary particle passing a specified cylindrical target volume of diameter D at a distance d from the cylinder's main axis. The shown track segment of the particle is represented by its ionization component.

density of the filling gas, on shape and size of the target volume, and on the distance d:

$$M_\xi(Q;d) = \sum_{v=0}^{\infty} v^\xi P_v(Q;d), \quad \text{with}$$

$$\sum_{v=0}^{\infty} P_v(Q;d) = 1. \tag{1}$$

The first moment $M_1(Q;d)$ stands for the mean cluster size, and the second moment $M_2(Q;d)$, for instance, is needed to determine the variance $M_2(Q;d) - M_1(Q;d)^2$ which characterizes the fluctuation of cluster-size formation.

To describe the cluster-size distribution $P_v(Q;d)$, De Nardo *et al.*[8] introduced (i) the probability $p_\kappa[\bar{\kappa}(Q)]$ that exactly κ primary ionizations are produced along a relevant path segment by a primary particle of quality Q provided that $\bar{\kappa}(Q)$ primary ionizations are generated on the average and (ii) the probability $f_v^{(\kappa)}(Q,d)$ that, including the contribution by secondary electrons, a cluster size v is caused at distance d from the particle path in the case of κ primary ionizations. As a result, the probability $P_v(Q;d)$ of the cluster size v being formed is given by the following equation:

$$P_v(Q;d) = \sum_{\kappa=0}^{\infty} p_\kappa[\bar{\kappa}(Q)]\, f_v^{(\kappa)}(Q,d). \tag{2}$$

Equation 2 represents a compound process of the same type as that discussed by Kellerer[9] and Kellerer and Chmelevsky[10], considering the distribution of specific energy produced in multiple energy deposition events. In the case of a homogeneous medium, the first factor of the summands of Equation 2 is independent of distance d, and stands for the formation of primary ionizations with a mean number $\bar{\kappa}(Q)$, which is directly proportional to the ionization cross section of a charged particle. If the relevant path segment is much smaller than the particle range, primary ionization events are statistically independent. In consequence, the number of primary ionizations is characterized by a poisson distribution for $p_\kappa[\bar{\kappa}(Q)]$, with a mean number $\bar{\kappa}(Q)$ of ionizations.

The second factor of the summands of Equation 2 represents the formation of the cluster size v at distance d from the particle path in the case of exactly a number κ of primary ionizations. By definition, it is independent of the stochastic nature of primary ionization, but depends on the stochastic nature of electron ejection in primary ionizations and of the subsequent electron degradation. Hence, it can be assumed that cluster-size formation as a result of κ independent primary ionizations is also statistically independent. In consequence, the probability $f_v^{(\kappa)}(Q,d)$ can be interpreted as the κ-fold convolution $[f_v^{(1)}(Q,d)]^{*\kappa}$ of the probability $f_v^{(1)}(Q,d)$ of the cluster size v being formed in the case of a single primary ionization.

If multiple ionization events and the production of Auger electrons are excluded, the $f_v^{(1)}(Q,d)$-distribution can be represented by Equation 3:

$$f_v^{(1)}(Q,d) = g_0(d) \times h_v(Q,d) + g_1(d) \times h_{v-1}(Q,d). \tag{3}$$

Here, $h_v(Q,d)$ is the cluster-size distribution exclusively due to secondary electrons, which are set in motion by primary particles of radiation quality Q passing the target cylinder at distance d. The parameters $g_0(d)$ and $g_1(d) = 1 - g_0(d)$ are geometry factors that represent the contribution of primary particle interactions. If D is the diameter of the target volume and a straight line is assumed for the primary particle's travelling route, $g_0(d)$ is given by:

$$g_0(d) = 1 - \sqrt{1 - \left(\frac{2d}{D}\right)^2} \quad \text{at } d \le \frac{D}{2} \quad \text{and}$$

$$g_0(d) = 1 \quad \text{at } d > \frac{D}{2}. \tag{4}$$

As a result, $g_0(d) = 0$ and $g_1(d) = 1$ at $d = 0$ stands for primary particles penetrating the target volume on one of its diameters, and $g_0(d) = 1$ and $g_1(d) = 0$ at $d > D/2$ is for primary particles passing aside the target. According to Equation 3, the resulting $f_v^{(1)}(Q,d)$-distributions are then given by $f_v^{(1)}(Q,d) = 0$ for $v = 0$ or $f_v^{(1)}(Q,d) = h_{v-1}(Q,d)$ for $v > 0$ at $d = 0$, and by $f_v^{(1)}(Q,d) = h_v(Q,d)$ at $d > D/2$. If there is no contribution to the ionization cluster size by secondary electrons, $h_v(Q,d)$ is always equal to one for $v = 0$, and equal to zero elsewhere. It should be mentioned that the extension of Equation 3 to also include multiple primary ionization events or Auger electron production is straightforward.

Now, inserting a poisson-like distribution for $p_\kappa[\bar{\kappa}(Q)]$ into Equation 2, the probability $P_v(Q;d)$ of cluster size v being formed at a distance d from the relevant particle path segment is given by

$$P_v(Q;d) = \sum_{\kappa=0}^{\infty} \frac{\mathrm{e}^{-\bar{\kappa}(Q)}\bar{\kappa}(Q)^\kappa}{\kappa!} [f_v^{(1)}(Q,d)]^{*\kappa} \tag{5}$$

in which $[f_v^{(1)}(Q,d)]^{*\kappa}$ is equal to $f_v^{(1)}(Q,d)$ at $\kappa = 1$, and equal to δ_{0v} at $\kappa = 0$. Equation 5 implies that the measured probability $P_v(Q;d)$ of cluster-size formation is definitely correlated with the probability $f_v^{(1)}(Q,d)$ of cluster-size formation in the case of a single primary ionization. For this reason, the moments $M_\xi(Q;d)$ of the distribution of $P_v(Q;d)$ are also related to the moments $m_\xi(Q,d)$ of the probability distribution $f_v^{(1)}(Q,d)$:

$$m_\xi(Q,d) = \sum_{v=0}^{\infty} v^\xi f_v^{(1)}(Q,d), \quad \text{with}$$

$$\sum_{v=0}^{\infty} f_v^{(1)}(Q,d) = 1. \tag{6}$$

As derived by De Nardo *et al.*[8], the moments $m_\xi(Q,d)$ of the single-ionization distribution $f_v^{(1)}(Q,d)$ are related to the cumulants $C_\xi(Q,d)$ of the compound process via the mean number $\bar{\kappa}(Q)$ of primary ionizations along a relevant path segment of a primary particle:

$$C_\xi(Q,d) = \bar{\kappa}(Q) \times m_\xi(Q,d). \quad (7)$$

Here, the first cumulant represents the mean cluster size $M_1(Q;d)$, and the second, the variance $M_2(Q;d) - M_1(Q;d)^2$.

As a result, the moments $M_\xi(Q;d)$ derived from measured $P_v(Q;d)$-distributions cannot be used to determine separately the moments $m_\xi(\mathrm{Q},d)$. They can, however, be used to determine the ratios of moments of a single-ionization distribution because these ratios are equal to the ratios of the corresponding cumulants $C_\xi(Q,d)$ of the $P_v(Q;d)$ distribution, which in turn are definitely determined by combinations of moments $M_\xi(Q;d)$. One of the most important examples of such ratios is given by Equation 8, which relates the variance $C_2(Q,d)$ to the mean cluster size:

$$\frac{C_2(Q,d)}{C_1(Q,d)} = \frac{M_2(Q;d)}{M_1(Q;d)} - M_1(Q;d) = \frac{m_2(Q,d)}{m_1(Q,d)}. \quad (8)$$

In a mixed notation, it follows from Equation 8 that the variance is directly proportional to the mean cluster size:

$$C_2(Q,d) = M_1(Q;d) \times \frac{m_2(Q,d)}{m_1(Q,d)}. \quad (9)$$

From the mathematical point of view, Equations 8 and 9 are formally equivalent to the expressions used in microdosimetry to relate the ratio of the variance of specific energy z to the absorbed dose, in the case of the dose-dependent microdosimetric distribution $f(z;d)$, with the single-event quantity dose-mean specific energy per event $\bar{z}_d$ [for a detailed discussion of these quantities, see again the publication by Kellerer [9]].

To give an impression on the cluster-size formation in liquid water, Figure 2 shows the probability $P_v(Q;d)$ of cluster size v calculated by Monte Carlo simulation for 5.4 MeV alpha particles penetrating a cylindrical volume with a diameter and height of mass per area $(D\rho)^{(\mathrm{water})}$, along a radius in the plane perpendicular to the cylinder's main axis at half its height (this irradiation geometry corresponds to a distance $d = 0$). The typical increase in the most probable cluster size by increasing its diameter is striking. For some details of the applied Monte Carlo model, see the publication by Grosswendt[11]. Figure 3 shows the mean cluster size $M_1(Q;d)$ for the same target volumes, yet as a function of the mass per area $d\rho$ of the distance between the cylinder's main axis and the centre line of the particle beam. The mean cluster size is greatest at $d = 0$, and decreases with increasing distance because of the decreasing travelling length of the particles within the target volume that leads to a reduction in the number of primary ionizations. At distances greater than the cylinder's radius, the ionization cluster size

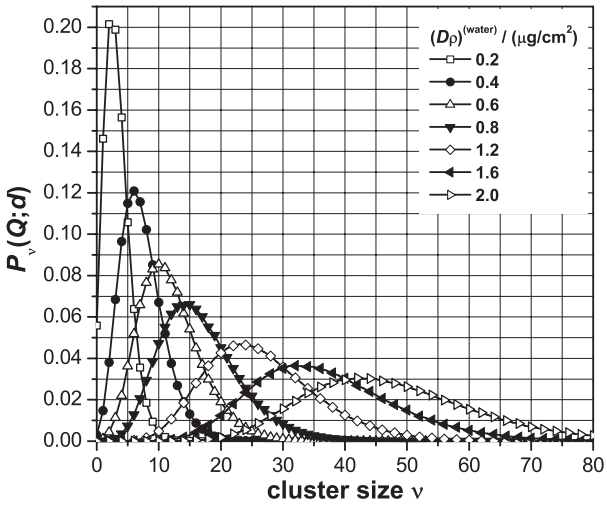

Figure 2. Probability $P_v(Q;d)$ of cluster size v in liquid water due to 5.4 MeV alpha particles penetrating a cylindrical volume with a diameter and height of mass per area $(D\rho)^{(\mathrm{water})}$, along a radius in the plane perpendicular to the cylinder's main axis at half its height (this irradiation geometry corresponds to a distance $d = 0$).

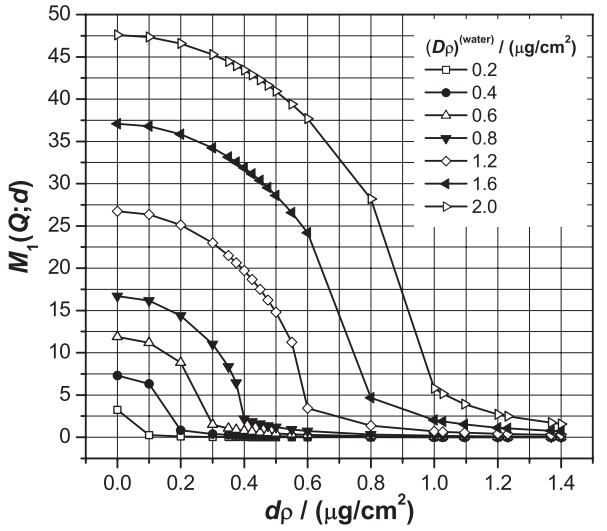

Figure 3. Mean ionization cluster size $M_1(Q;d)$ for the target volumes of Figure 2 as a function of the mass per area $d\rho$ of the distance between the cylinder's main axis and the centre line of the particle beam; the mass per area $(D\rho)^{(\mathrm{water})}$ of the target diameter and height is used as a parameter.

is exclusively determined by the contribution due to secondary electrons.

In the special case of charged particles at initial energy T, which are completely absorbed in a macroscopic target volume, the mean cluster size $M_1(Q;d)$ is independent of d by definition and equal to the mean number $N(T)$ of ion pairs formed. $N(T)$ is conventionally expressed by the ratio of the energy T to the mean energy $W(T)$ required to form an ion pair upon the complete degradation of a charged particle in a gas[12]. Bearing in mind a typical microdosimetric experiment, the mean ionization cluster size of a charged particle at energy T, which crosses a detector volume, is equal to the ratio of its energy loss ΔT to the differential value $\omega(T)$ of the mean energy required to produce an ion pair if ΔT is completely absorbed within the detector. Here, $\omega(T)$ is defined as the quotient dT/dN, where dT is the mean energy lost by a charged particle at energy T while traversing an absorber of specified thickness, and dN is the mean number of ion pairs produced if dT is completely dissipated in the detector gas[12]. In contrast to macroscopic targets, however, none of the necessary conditions for the validity of $W(T)$ or $\omega(T)$ are fulfilled in target volumes of nanometric dimensions, and the mean ionization cluster sizes are determined by the compound process of primary impact ionization and of secondary electron transport. If the latter can be neglected, the mean cluster size of a particle at energy T exclusively depends on the ratio of the primary particle's track length L within a target to its mean free path length $\lambda_{ion}(T)$ with respect to primary ionization. As $\lambda_{ion}(T)$ is proportional to the reciprocal of the ionization cross section $\sigma_{ion}(T)$, the mean cluster size $M_1(T;L)$ is proportional to $\sigma_{ion}(T)$. To give an impression of such data, Figure 4 shows the ionization cross section of liquid water for electrons, protons and alpha particles as a function of energy T, where the energy T_{proj} of the heavier projectiles is represented by the energy of electrons at the same velocity: $T = (m_{el}/m_{proj}) \times T_{proj}$ (m_{el} is the electron mass and m_{proj} is the mass of the projectile). The cross sections for electrons were taken from Dingfelder *et al.*[13] whereas those of the light ions were calculated using the data of Rudd *et al.*[14] for protons at the same velocity and applying the scaling and correction procedure described by Grosswendt[11]. As is obvious from Figure 4, the data for electrons at energies greater than about 500 eV are almost the same as those of protons at the same velocity, but they are markedly smaller at lower energies. The data for the alpha particles at higher energies are greater than those of protons by approximately a factor of four due to the quadratic dependence of $\sigma_{ion}(T)$ on the projectile's atomic number. It should, however, be noted that the cross section of electron at ~100 eV is comparable with the cross section of alpha particles at higher energies, demonstrating the great ionization capability of low-energy electrons.

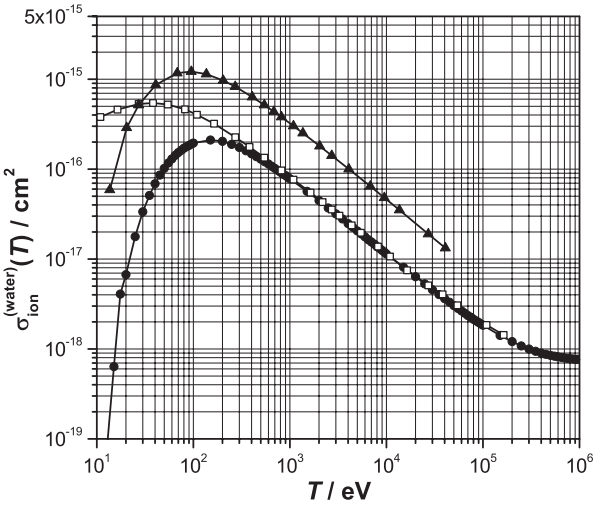

Figure 4. Ionization cross section $\sigma_{ion}^{(water)}(T)$ of liquid water for electrons, protons and alpha particles as a function of energy T. The energy of the heavier projectiles, T_{proj}, is represented by the energy of electrons at the same velocity: $T = (m_{el}/m_{proj}) \times T_{proj}$ (m_{el} is the electron mass, and m_{proj} is the projectile mass): electrons (●), protons (□) and bare He ions (▲).

NANODOSIMETRIC MEASURING DEVICES

Figure 5 shows the principle which can be applied to measure ionization cluster-size distributions in radiation-sensitive biological volumes. A charged particle beam enters a gas-filled interaction chamber, penetrates through or passes aside a wall-less target volume of definite shape and size, and reaches a trigger detector. Ions or low-energy electrons induced directly by each primary particle or by its secondaries within the target volume are extracted from the interaction chamber into an evacuated drift chamber and detected by an ion or electron counter, which is able to detect single particles. This measuring principle is based on the idea of experimental microdosimetry that the sizes of a gas-filled measuring volume expressed in mass per area must be the same as those of the simulated target of liquid water, as a substitute to a sub-cellular biological target. In order to simulate, for instance, a cylindrical volume of liquid water, 2 nm in diameter, by a gaseous volume, 1 mm in diameter, the gas density must be 2 μg cm^{-3} which corresponds to a gas pressure of the order of 1 mbar. Applying this method, it is assumed that (i) the interaction mechanisms of ionizing radiation in the counter gas are similar to those in tissue-equivalent matter, (ii) the interaction cross sections and the number or kind of the most important energy loss channels are almost independent of gas

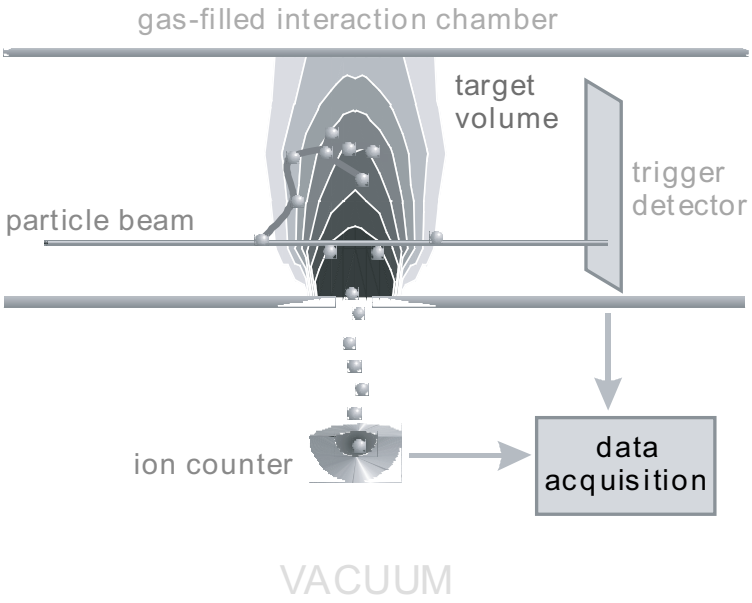

Figure 5. Schematic view of a typical ion-counting measuring device which can be applied for determining ionization cluster-size distributions.

density, and (iii) the particle tracks are not noticeably disturbed by any component of the measuring device.

Ion-counting measuring devices

The nanodosimeter at the Weizmann Institute of Science

In the nanodosimetric experiments performed at the Weizmann Institute [Garty *et al.*[7]], a projectile particle beam (from an accelerator or an alpha particle source) is degraded and collimated to a specified energy and irradiation geometry. It then traverses a detection volume of propane from which ions can be extracted, and reaches a trigger detector. Ions induced in the detection volume are extracted into vacuum and detected by an ion counter. The data acquisition system registers arrival time of the ions at the counter with respect to the trigger. These data are used afterwards to determine the frequency of ionization cluster size.

The size and shape of the wall-less detection volume are determined by the extraction efficiency of ions through an aperture, and depend on gas density, aperture diameter and the electric fields above and below the ion extraction aperture. In consequence, the sensitive volume is represented by a map of tapered, cylindrically symmetrical volume-contours representing equal ion-extraction efficiencies. These maps were determined by calculations based on the electric field geometry of the measuring device and on measured ion-transport parameters. The size of the sensitive volume, at unit density, is parameterized by the 50% contour of the ion-extraction efficiency. In a typical measurement using propane, the diameter of the 50% efficiency contour corresponds to 3.7 nm and its height to 90 nm. Smaller sensitive volumes can, however, easily be reached by reducing the gas pressure or by restricting the arrival time of the ions at the detector.

The Jet counter at the Soltan Institute of Nuclear Studies

In the Jet Counter at the Soltan Institute [Pszona *et al.*[5]], the gas cavity which simulates a nanometric volume at unit density is obtained by pulse expansion of a gas (for instance, nitrogen) into an interaction chamber, leading to a pulsed jet of gas molecules. The volume of the interaction chamber is of cylindrical shape, 10 mm in diameter and 15 mm in height, with walls made of stainless steel (or tissue-equivalent material if necessary). Pulse expansion is performed by means of a fast piezoelectric valve, which is connected to a second valve and injects the gas through a nozzle with an orifice, 1 mm in diameter, from a reservoir into the interaction chamber below the nozzle. This interaction chamber is subdivided into two cavities separated by a grid. The cavity between the grid and the open bottom of the interaction chamber represents the simulated nanometre-sized site from which ions can be collected with known detection efficiency. In the end, this cavity forms a cylindrical target volume of equal height and diameter. In a typical experiment with 4.6 MeV alpha particles, the mass per area of the volume's diameter and height was varied between about 0.1 and 1.3 μg cm^{-2}, using jets of molecular nitrogen. Here, the detection efficiency of

the counter decreased with increasing mass per area from about 50% to 40%.

Electron-counting measuring devices

The track-nanodosimetric counter of Laboratori Nazionali di Legnaro

The track-nanodosimetric counter at Laboratori Nazionali di Legnaro [De Nardo *et al.*[6]] is the only one at present which is capable of measuring the probability distribution of ionization cluster-size formation in nanometric volumes as a function of the distance from the centre line of a primary particle beam. In addition, it is also the only one which is based on the principle of single-electron detection and counts single electrons at very low gas pressure without being affected by gas gain fluctuations.

The nanodosimetric counter essentially consists of an electron collector and a single-electron counter. The electron collector is formed by a system of electrodes which enclose an almost wall-less millimetric volume, representing the sensitive volume of the counter. The shape of this volume is that of a cylinder, the height of which is equal to its diameter (3.7 mm). In typical experiments with 5.4 MeV alpha particles, propane was used as the detector gas. In this case, the diameter of the sensitive volume had a mass per area of about 2 μg cm^{-2} which corresponds to 20 nm at unit density. Electrons generated within the sensitive volume by ionizing interactions are transferred into the single-electron counter, which consists of a long cylindrical drift column and an electron multiplier. This electron multiplier uses the measuring principle applied by convention in multistep avalanche chambers. Electrons created inside the sensitive volume enter the drift column of the single-electron counter and arrive at the multistep avalanche chamber at different time intervals. Here, each single electron generates an electronic avalanche which is used to produce a detectable signal. Since each signal, independent of its height, is considered to represent one electron, the fluctuation of the amplification (gas gain) is not important. Each electron cluster collected from the sensitive volume gives rise to a pulse trail which is used to count the number of ionizations in a cluster. At present, there is an efficiency of the counter of about ~25%.

EQUIVALENCE OF IONIZATION CLUSTER-SIZE DISTRIBUTIONS

As discussed in the introduction, one of the challenges of radiation metrology is to be able to determine ionization cluster-size distributions due to ionizing radiation in nanometric target volumes of liquid water, as a substitute to sub-cellular radiosensitive biological targets. This challenge is tackled in nanodosimetry by measuring ionization cluster-size distributions in gaseous target volumes, the sizes of which are comparable in mass per area to those of sub-cellular targets. At first glance, this procedure seems to be of doubtful value since it is hardly conceivable that gaseous systems well suited for proportional counter experiments show the same mechanisms of radiation interaction as sub-cellular material. This argument is generally true as seen at excitation processes which strongly depend on the target species, but it is not so serious from the point of view of ionization cluster-size formation because the energy distribution of secondary electrons set in motion by impact ionization does not strongly depend on the type of target molecules.

To study the material equivalence regarding the formation of ionization cluster size, let us assume a cylindrical gaseous target of diameter D and mass per area $(D\rho)^{(\mathrm{gas})}$ which is passed by a charged particle of radiation quality Q at a distance d from the cylinder's main axis in a plane at half its height. According to Equation 7, the mean ionization cluster size (including the contribution by secondary electrons) is given by the following equation:

$$M_1^{(\mathrm{gas})}(Q;d) = \bar{\kappa}^{(\mathrm{gas})}(Q) \times m_1^{(\mathrm{gas})}(Q,d) = \frac{(D\rho)^{(\mathrm{gas})}}{(\lambda\rho)_{\mathrm{ion}}^{(\mathrm{gas})}(Q)} \times m_1^{(\mathrm{gas})}(Q,d), \qquad (11)$$

where $M_1^{(\mathrm{gas})}(Q;d)$ is the first moment of the ionization cluster-size distribution in the gas at distance d, $(\lambda\rho)_{\mathrm{ion}}^{(\mathrm{gas})}(Q)$ is the mass per area of the particle's mean free path length with respect to ionization of the target gas, and $m_1^{(\mathrm{gas})}(Q,d)$ is the first moment of the single-ionization distribution in the gas. Without reservation of generality, the mean number $\bar{\kappa}^{(\mathrm{gas})}(Q)$ of ionizations due to primary interactions in the gas was set equal to the ratio of $(D\rho)^{(\mathrm{gas})}/(\lambda\rho)_{\mathrm{ion}}^{(\mathrm{gas})}(Q)$.

One constraint on the validity of cluster-size distributions measured in gaseous systems for determining cluster-size distributions in cylindrical volumes of liquid water is the requirement that, at least, the mean cluster sizes in both systems are the same. Applying Equation 11 also to the first moment of the $P_\nu(Q;d)$-distribution in a cylinder of liquid water with a diameter of mass per area $(D\rho)^{(\mathrm{water})}$, the condition for equal mean cluster sizes $M_1^{(\mathrm{gas})}(Q;d) = M_1^{(\mathrm{water})}(Q;d)$ is given by

$$(D\rho)^{(\mathrm{gas})} = (D\rho)^{(\mathrm{water})} \times \frac{(\lambda\rho)_{\mathrm{ion}}^{(\mathrm{gas})}(Q)}{(\lambda\rho)_{\mathrm{ion}}^{(\mathrm{water})}(Q)} \times \frac{m_1^{(\mathrm{water})}(Q,d)}{m_1^{(\mathrm{gas})}(Q,d)}, \qquad (12)$$

which relates the diameter of the water cylinder to the equivalent diameter of the gaseous system via a

scaling parameter. This scaling parameter is defined by the product of the ratio of the mass per area of the mean free ionization path length in the gas to that in water and of the ratio of the first moment of the single-ionization distribution in water to that in gas. It can be expected that a gaseous target cylinder with a diameter of mass per area $(D\rho)^{(\mathrm{gas})}$ calculated according to Equation 12 leads to the same mean cluster size as a target cylinder of liquid water with a diameter of specified mass per area $(D\rho)^{(\mathrm{water})}$.

A further constraint on the validity of cluster-size distributions measured in gaseous systems for determining cluster-size distributions in cylindrical volumes of liquid water is the requirement that also the variances in both systems are, at least, approximately the same. The variance $C_2^{(\mathrm{gas})}(Q,d)$ of the $P_\nu(Q;d)$-distributions with respect to a gaseous cylinder volume of diameter $(D\rho)^{(\mathrm{gas})}$ can be calculated using Equation 7 again and inserting for $\bar{\kappa}^{(\mathrm{gas})}(Q)$ the ratio $(D\rho)^{(\mathrm{gas})}/(\lambda\rho)_{\mathrm{ion}}^{(\mathrm{gas})}(Q)$ of Equation 12. After applying Equation 7 also to a cylinder of liquid water with a diameter of mass per area $(D\rho)^{(\mathrm{water})}$ and after some reordering of quantities, the variance for the gaseous system can be related to that of liquid water in the following way:

$$C_2^{(\mathrm{gas})}(Q,d) = C_2^{(\mathrm{water})}(Q,d) \times \frac{m_1^{(\mathrm{water})}(Q,d)}{m_1^{(\mathrm{gas})}(Q,d)} \times \frac{m_2^{(\mathrm{gas})}(Q,d)}{m_2^{(\mathrm{water})}(Q,d)}. \qquad (13)$$

Hence, it can also be stated that the variance in the case of the scaled gaseous cylinder is the same as that for the cylinder of liquid water if the moment ratios $m_1^{(\mathrm{water})}(Q,d)/m_1^{(\mathrm{gas})}(Q,d)$ and $m_2^{(\mathrm{water})}(Q,d)/m_2^{(\mathrm{gas})}(Q,d)$ are equal to one. This condition means that the behaviour of secondary electrons in the two media must be similar, which, however, is generally not the case.

As a result of Equations 12 and 13, which are valid without restrictions, it is obvious that a material equivalence which is exclusively based on the mass per area of target sizes only exists if the spectral distribution of secondary electrons, the energy degradation of these secondaries and the mass per areas of the mean free ionization path lengths of the primary particles in gas and in liquid water are the same.

Unfortunately, Equations 12 and 13 can only be used if the first and second moments of the single-ionization distributions in gas and in liquid water are known, for instance, by a series of Monte Carlo calculations. They can, however, be directly applied if the contribution of secondary electrons to the cluster-size distributions in both media is negligible. For this purpose, it is assumed (i) that the primary particles penetrate a target cylinder on a radius in the plane perpendicular to the target axis at half its height (which corresponds to the distance $d = 0$), and (ii) that the diameter and height of the target volume are much smaller than the range of secondary electrons. The latter condition implies that the contribution of secondary electrons to ionization cluster size can be neglected. Both assumptions together lead to single-ionization distributions $f_\nu^{(1)}(Q,d)$ at $d = 0$ which are equal to one for $\nu = 1$ and equal to zero elsewhere [see the remarks on $f_\nu^{(1)}(Q,d)$-distributions in the section concerning the general aspects of ionization cluster-size formation]. In consequence, the moments $m_1(Q,d)$ and $m_2(Q,d)$ of the $f_\nu^{(1)}(Q,d)$-distributions are also equal to one, at $d = 0$. This leads to a very simple scaling procedure to reach material equivalence, which is based only on the parameters of primary ionization:

$$(D\rho)^{(\mathrm{gas})} = (D\rho)^{(\mathrm{water})} \times \frac{(\lambda\rho)_{\mathrm{ion}}^{(\mathrm{gas})}(Q)}{(\lambda\rho)_{\mathrm{ion}}^{(\mathrm{water})}(Q)}. \qquad (14)$$

In the case of a negligible contribution of secondary electrons to cluster-size formation, a gaseous cylinder of diameter D with a mass per area $(D\rho)^{(\mathrm{gas})}$ calculated according to Equation 14 would lead to the same mean cluster size and to the same variance as a cylindrical volume of liquid water with a diameter of mass per area $(D\rho)^{(\mathrm{water})}$.

The mean free path lengths $(\lambda\rho)_{\mathrm{ion}}^{(\mathrm{nitrogen})}$ and $(\lambda\rho)_{\mathrm{ion}}^{(\mathrm{propane})}$ of alpha particles with respect to ionization in nitrogen or propane are presented in Figure 6 as a function of energy T, in comparison with those in liquid water. At first glance, it can be seen from the figure that $(\lambda\rho)_{\mathrm{ion}}^{(\mathrm{nitrogen})}$ is always greater than $(\lambda\rho)_{\mathrm{ion}}^{(\mathrm{water})}$, whereas $(\lambda\rho)_{\mathrm{ion}}^{(\mathrm{propane})}$ is always smaller than $(\lambda\rho)_{\mathrm{ion}}^{(\mathrm{water})}$. In consequence, the mass per area

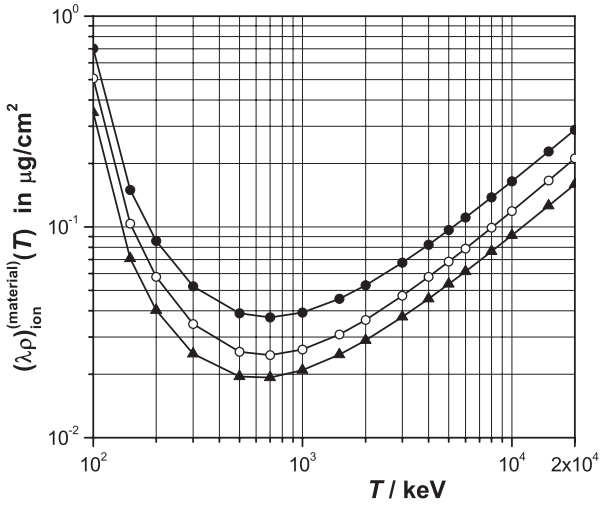

Figure 6. Mean free ionization path lengths $(\lambda\rho)_{\mathrm{ion}}^{(\mathrm{material})}$ of alpha particles in nitrogen, liquid water or propane as a function of the particle energy T: nitrogen (●), liquid water (○) and propane (▲).

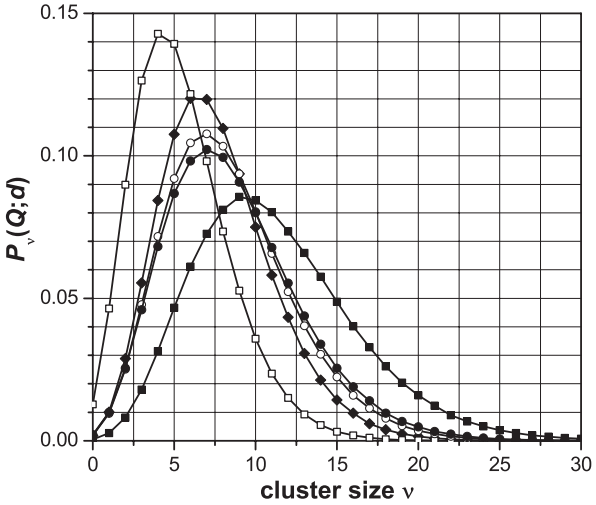

Figure 7. Ionization cluster-size distributions $P_\nu(Q;d)$ for 4.6 MeV alpha particles penetrating cylindrical volumes of nitrogen, liquid water or propane at distance $d = 0$ in the plane perpendicular to the cylinder's main axis at half its height, with the mass per area $(D\rho)$ of the cylinder's diameter as a parameter. $(D\rho) = 0.4$ μg cm^{-2}: liquid water (◆), nitrogen (□) and propane (■); scaled mass per area using Equation 14: $(D\rho) = 0.578$ μg cm^{-2} for nitrogen (○), $(D\rho) = 0.321$ μg cm^{-2} for propane (●).

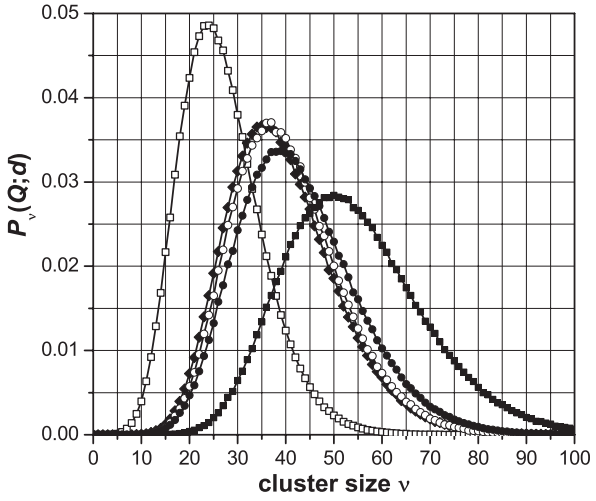

Figure 8. Ionization cluster-size distributions $P_\nu(Q;d)$ for 4.6 MeV alpha particles as in Figure 7, but at a greater mass per area of the diameter. $(D\rho) = 1.6$ μg cm^{-2}: liquid water (◆), nitrogen (□) and propane (■); scaled mass per area using Equation 14: $(D\rho) = 2.31$ μg cm^{-2} for nitrogen (○), $(D\rho) = 1.28$ μg cm^{-2} for propane (●).

of the equivalent diameter in nitrogen is greater than that specified for water, whereas in propane, it always is smaller.

To demonstrate the validity of the approximate scaling procedure defined by Equation 14, Monte Carlo simulations were performed to calculate the ionization cluster-size distributions for alpha particles penetrating cylindrical volumes of nitrogen, liquid water or propane at distance $d = 0$, in the plane perpendicular to the cylinder's main axis at half its height, which was equal to the diameter. The mass per area of the diameter was varied between 0.2 and 2.0 μg cm^{-2}. For liquid water, the simulations were based on the model of Grosswendt[11]; for propane, on that of De Nardo *et al.*[8]; and for nitrogen, on that of Grosswendt and Pszona[15]. Figure 7 shows the results for alpha particles at 4.6 MeV. Five $P_\nu(Q;d)$-distributions are presented, three of them with a mass per area of the target diameter of 0.4 μg cm^{-2} and the other two with the scaled mass per areas $(D\rho)^{(\text{nitrogen})}$ and $(D\rho)^{(\text{propane})}$ for nitrogen and propane according to Equation 14, using the data of Figure 6. The corresponding distributions for larger diameters of the target volumes are presented in Figure 8. It is obvious from both figures that the cluster-size distributions, in volumes of propane or nitrogen with diameters of mass per area equal to that of a liquid water target, are very different, whereas the $P_\nu(Q;d)$-distributions for the volumes with a diameter scaled according to Equation 14 are rather similar. It can, therefore, be stated that measurements in gases can be used to determine ionization cluster-size distributions also in specified nanometric volumes of liquid water if the sizes of the target volumes in the gas are chosen appropriately.

THE RELATION OF IONIZATION CLUSTER-SIZE DISTRIBUTIONS TO RADIATION BIOLOGY

As mentioned in the introduction, the yields of clusters of multiple ionization in sites, 2–3 nm in size, correlate well with observed yields of double-strand breaks of DNA[4]. In consequence, it can be expected that the probability of cluster-size formation in nanometric volumes of liquid water for sizes $\nu \geq 2$ behaves as a function of radiation quality, like radiation damage to sub-cellular structures, at least, for particular endpoints.

As extensively discussed by Simmons and Watt[16], radiation damage due to electrons and X rays can be expressed for various endpoints by the bio-effect cross section $\sigma_B(\lambda_{ion})$ given by Equation 15 as a function of the mean free path length with respect to primary ionization:

$$\sigma_B(\lambda_{ion}) = 3[1 - e^{-0.36\ \mu g\ cm^{-2}/(\lambda\rho)_{ion}}]^2 \times 10^{-8} cm^2. \quad (15)$$

To check the assumption that the probability of cluster-size formation for sizes $\nu \geq 2$ behaves like

radiation damage, the distribution function $F_k(Q) = \sum_{v=k}^{\infty} P_v(Q;d)$ of the $P_v(Q;d)$-distribution for $v \geq k$ could be used at $k = 2$. For this purpose, the cluster size distribution $P_v(Q;d)$ was calculated for electrons as a function of energy T, as a substitute of the radiation quality Q, for a cylindrical volume with a diameter and height of mass per area 0.2 μg cm^{-2} in liquid water, using the Monte Carlo model of Grosswendt[11]. Here, it was assumed that the primary electrons penetrate the target cylinder at distance $d = 0$ in the plane perpendicular to the target's main axis at half its height. Figure 9 shows the results as regards the distribution functions $F_k(T)$ for $k = 1$, 2, 3 or 5 plotted as a function of energy $T-(k-1) \times I_{\text{ion}}$ which represents the highest possible electron energy after $(k-1)$ ionizing interactions (I_{ion} is the lowest ionization threshold energy of liquid water). As expected, the distribution function $F_k(T)$ is highest for $k = 1$ and decreases with increasing value k of the smallest cluster size taken into account. As far as the energy dependence is concerned, $F_k(T)$ strongly increases with increasing electron energy at the low-energy side, reaches a maximum at ~150 eV, and decreases afterwards if the energy is further increased. The steep increase at lower energies is caused (i) by a strong reduction of the mean free ionization path length $(\lambda\rho)_{\text{ion}}^{(\text{water})}(T)$ with rising energy, and (ii) by fact that low-energy electrons are only able to produce small cluster sizes, as their energy is degraded to values below the ionization threshold after a small number of interactions which increases with rising energy. In contrast, the strong reduction of $F_k(T)$ at higher energies is due to the increase in $(\lambda\rho)_{\text{ion}}^{(\text{water})}(T)$ of electrons, which leads to a distance between successive ionizing interactions that is greater than the sizes of the target volume. The maximum value of the distribution functions occurs at an electron energy of ~150 eV where $(\lambda\rho)_{\text{ion}}^{(\text{water})}(T)$ is smallest.

In order to test the applicability of distribution functions $F_k(T)$ to radiation biology, the bioeffect cross section $\sigma_B(\lambda_{\text{ion}})$ of Simmons and Watt was first calculated as a function of energy, using the mean free ionization path length $(\lambda\rho)_{\text{ion}}^{(\text{water})}(T)$ of electrons at $T - I_{\text{ion}}$ in liquid water (derived from the ionization cross sections of Figure 4). Afterwards, the probability $F_2(T)$ of at least two ionizations was scaled to $\sigma_B(\lambda_{\text{ion}})$ at an electron energy of 150 eV, which is the energy of the minimal mean free ionization path length $(\lambda\rho)_{\text{ion}}^{(\text{water})}(T)$. Figure 10 shows the energy dependence of these scaled values in comparison with the bio-effect cross section. At first glance, it can be seen that the energy dependence of the bio-effect cross section and that of the scaled probability $F_2(T)$ for primary electrons in cylindrical volumes of mass per area 0.2 μg cm^{-2} in diameter and height are quite similar. The use of cluster-size distributions for scaling radiobiological effects, therefore, seems to be promising, at least, for particular endpoints. In this respect, see also the

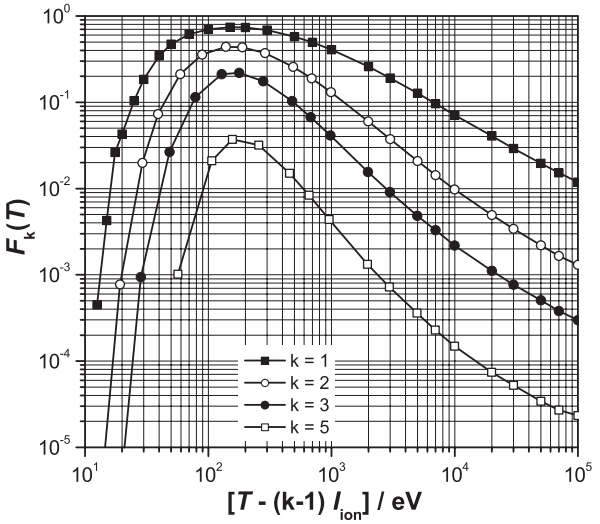

Figure 9. Distribution functions $F_k(T)$ for $k = 1$, 2, 3 or 5 plotted as a function of the energy $T-(k-1) \times I_{\text{ion}}$ of primary electrons in liquid water (I_{ion} lowest ionization threshold energy). The electrons penetrate the target volume, which is a cylinder of equal diameter and height of mass per area 0.2 μg cm^{-2}, at distance $d = 0$ in the plane perpendicular to the target's main axis at half its height.

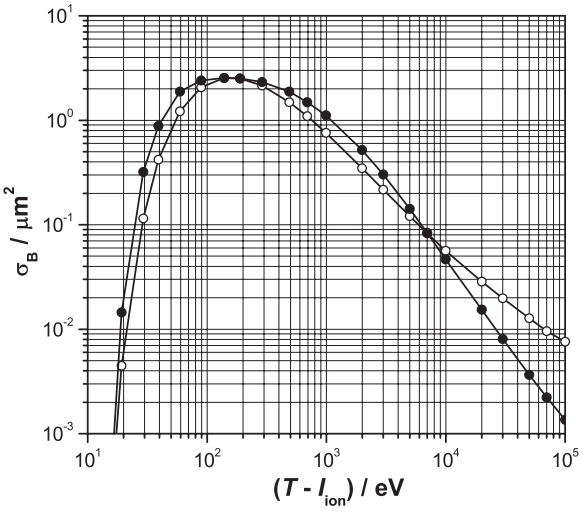

Figure 10. Bio-effect cross section $\sigma_B(\lambda_{\text{ion}})$ for primary electrons as a function of energy $T - I_{\text{ion}}$ (I_{ion} lowest ionization threshold energy of liquid water): cross section of Simmons and Watt[16] given by Equation 15 using the mean free ionization path lengths $(\lambda\rho)_{\text{ion}}(T)$ of electrons in liquid water (●), distribution function $F_2(T)$ for electrons in liquid water (see Figure 9) scaled to the cross section of Simmons and Watt at 150 eV (○).

discussion of Grosswendt[17] with respect to the relation of ionization cluster-size formation and the track structure of photons, electrons and alpha particles.

REFERENCES

1. Goodhead, D. T. *Initial events in the cellular effects of ionizing radiations: clustered damage in DNA.* Int. J. Radiat. Biol. **65**(1), 7–17 (1994).
2. Nikjoo, H., O'Neill, P., Terrissol, M. and Goodhead, D. T. *Quantitative modelling of DNA damage using Monte Carlo track structure method.* Radiat. Environ. Biophys. **38**, 31–38 (1999).
3. Friedland, W., Jacob, P., Paretzke, H. G. and Stork, T. *Monte Carlo simulation of the production of short DNA fragments by low-linear energy transfer radiation using higher-order DNA models.* Radiat. Res. **150**, 170–182 (1998).
4. Brenner, D. J. and Ward, J. F. *Constraints on energy deposition and target size of multiply damaged sites associated with DNA double-strand breaks.* Int. J. Radiat. Biol. **61**(6), 737–748 (1992).
5. Pszona, S., Kula, J. and Marjanska, S. *A new method for measuring ion clusters produced by charged particles in nanometre track sections of DNA size.* Nucl. Instrum. Meth. Phys. Res. A **447**, 601–607 (2000).
6. De Nardo, L., Alkaa, A., Khamphan, C., Conte, V., Colautti, P., Ségur, P. and Tornielli, G. *A detector for track-nanodosimetry.* Nucl. Instrum. Meth. Phys. Res. A **484**, 312–326 (2002).
7. Garty, G., Shchemelinin, S., Breskin, A., Chechik, R., Assaf, G., Orion, I., Bashkirov, V., Schulte, R. and Grosswendt, B. *The performance of a novel ion-counting nanodosimeter.* Nucl. Instrum. Meth. Phys. Res. A **492**, 212–235 (2002).
8. De Nardo, L., Colautti, P., Conte, V., Baek, W. Y., Grosswendt, B. and Tornielli, G. *Ionization-cluster distributions of α-particles in nanometric volumes of propane: measurement and calculation.* Radiat. Environ. Biophys. **41**, 235–256 (2002).
9. Kellerer, A. M. *A survey of theoretical relations in microdosimetry.* In: Proceedings of the Second Symposium on Microdosimetry. Stresa, October 1969. Commission of the European Communities, Brussels, EUR 4452 d-f-e, pp. 107–134 (1970).
10. Kellerer, A. M. and Chmelevsky, D. *Concepts of microdosimetry—II. Probability distributions of the microdosimetric variables.* Radiat. Environ. Biophys. **12**, 205–216 (1975).
11. Grosswendt, B. *Formation of ionization clusters in nanometric structures of propane-based tissue-equivalent gas or liquid water by electrons and α-particles.* Radiat. Environ. Biophys. **41**, 103–112 (2002).
12. International Commission on Radiation Units and Measurements. *Average energy required to produce an ion pair.* ICRU Report 31. (Bethesda, MD: ICRU) (1979).
13. Dingfelder, M., Hantke, D., Inokuti, M. and Paretzke, H. G. *Electron inelastic-scattering cross sections in liquid water.* Radiat. Phys. Chem. **53**(1), 1–18 (1998).
14. Rudd, M. E., Goffe, T. V., DuBois, R.D. and Toburen, L. H. *Cross sections for ionization of water vapor by 7-4000-keV protons.* Phys. Rev. A **31**(1), 492–494 (1985).
15. Grosswendt, B. and Pszona, S. *The track structure of α-particles from the point of view of ionization-cluster formation in 'nanometric' volumes of nitrogen.* Radiat. Environ. Biophys. **41**, 91–102 (2002).
16. Simmons, J. A. and Watt, D. E. *Radiation Protection Dosimetry, A Radical Reappraisal.* Medical Physics Publishing, Madison, WI, (1999) ISBN 0-944838-87-1.
17. Grosswendt, B. *The track structure of photons, electrons and α-particles from the point of view of the formation of ionization clusters.* In: Proceedings of Conference—Advanced Monte Carlo for Radiation Physics, Particle Transport Simulation and Applications. Lisbon, October 2000, (Berlin, Heidelberg, New York: Springer-Verlag) pp. 237–250 (2001).